Interlayer correlation between two ^{4}He monolayers adsorbed on both sides of α-graphyne

Jeonghwan Ahn, Sungjin Park, Hoonkyung Lee, and Yongkyung Kwon*
Division of Quantum Phases and Devices, School of Physics, Konkuk University, Seoul 143-701, Korea
(Received 15 April 2015; revised manuscript received 11 June 2015; published 1 July 2015)

Path-integral Monte Carlo calculations have been performed to study the ^{4}He adsorption on both sides of a single α-graphyne sheet. For investigation of the interlayer correlation between the upper and the lower monolayers of ^{4}He adatoms, the ^{4}He-substrate interaction is described by the sum of the ^{4}He-C interatomic pair potentials for which we use both Lennard-Jones and Yukawa-6 anisotropic potentials. When the lower ^{4}He layer is a $C_{4/3}$ commensurate solid, the upper-layer ^{4}He atoms are found to form a kagome lattice structure at a Mott-insulating density of 0.0706 Å^{-2} and a commensurate solid at an areal density of 0.0941 Å^{-2} for both substrate potentials. The correlation between upper- and lower-layer pseudospins, which were introduced in Kwon *et al.* [Phys. Rev. B **88**, 201403(R) (2013)] for two degenerate configurations of three ^{4}He atoms in a hexagonal cell, depends on the substrate potential used; with the substrate potential based on the anisotropic Yukawa-6 pair potentials, the Ising pseudospins of both ^{4}He layers are found to be antiparallel to each other whereas the parallel and antiparallel pseudospin alignments between the two ^{4}He layers are nearly degenerate with the Lennard-Jones potentials. This is attributed to the difference in the interlayer distance, which is $\sim$4 Å with the Yukawa-6 substrate potential but as large as $\sim$4.8 Å with the Lennard-Jones potential.

DOI: 10.1103/PhysRevB.92.035402 PACS number(s): 67.25.bd, 67.25.bh, 67.80.B−

I. INTRODUCTION

Among many substrates, graphite has long served as a test bed to investigate low-dimensional quantum fluids because of its strong binding of adsorbates. Up to seven distinct ^{4}He layers were observed on graphite, and each helium layer is considered to be a quasi-two-dimensional quantum system [1]. The first ^{4}He adlayer on graphite shows a commensurate-incommensurate solid transition as the helium coverage increases [2–4]. Recently, a series of theoretical calculations has been performed to study the ^{4}He adsorption on newly synthesized (or proposed) low-dimensional carbon substrates, such as graphene [5–7], graphynes [8,9], carbon nanotubes [10,11], and fullerene molecules [12–15]. The phase diagrams of the ^{4}He layers adsorbed on graphene were predicted to be very similar to those of the corresponding layers on graphite; the monolayer of the ^{4}He adatoms shows a $C_{1/3}$ commensurate structure at the areal density of 0.0636 Å^{-2} and goes through various domain-wall phases before crystallizing into an incommensurate triangular solid near its completion [6,7,16].

Graphyne is a two-dimensional (2D) network of sp- and sp^2-bonded C atoms [17,18] which could be permeable to a ^{4}He gas unlike graphene. Despite much experimental effort motivated by some promising theoretical predictions for graphyne as new Dirac materials [19–21] and high-capacity energy storage materials [22–24], there has been no successful report yet for the fabrication of extended 2D graphynes. However, some flakes or building blocks of finite-size graphynes have been synthesized [25–27], leading to a belief that graphynes will be fabricated in the near future. On the surface of γ-graphyne, which is the most stable graphyne structure according to quantum Monte Carlo calculations [28], the ^{4}He monolayer was predicted to exhibit a richer phase diagram than the corresponding layer on graphene or graphite, including various commensurate and incommensurate structures depending on the helium density [9]. Recently one of us performed path-integral Monte Carlo (PIMC) calculations for ^{4}He atoms adsorbed on an AB-stacked bilayer α-graphyne [8], which is a hybridized honeycomb structure with each hexagon side consisting of one sp^2 and two sp C atoms. It was found that the ^{4}He monolayer was in a Mott-insulating state at an areal density of 0.0706 Å^{-2}, whereas a commensurate solid was realized at 0.0941 Å^{-2}. Introducing Ising pseudospin degrees of freedom for two degenerate configurations for three ^{4}He atoms occupying a hexagonal cell (see Fig. 3 of Ref. [8]), this Mott-insulator to commensurate-solid transition was interpreted as a symmetry-breaking process from a spin liquid of geometrically frustrated antiferromagnets to a spin-aligned ferromagnet [8].

One interesting feature of a 2D carbon structure, such as graphene and graphyne, is that it can be suspended in the air [29] and ^{4}He atoms can be coated on both sides. Noting that some new physics could emerge as a result of interlayer correlation between opposite-side ^{4}He layers, some theoretical studies were recently performed for the ^{4}He adsorption on both sides of a single graphene sheet. Vranješ Markić *et al.* found that the correlation between two ^{4}He clusters adsorbed on opposite sides of graphene, 5 to 6 Å apart from each other, was quite weak as evidenced by peakless pair distribution functions [30]. A weak correlation between two ^{4}He systems on the opposite sides of graphene was also predicted by Gordillo's diffusion Monte Carlo calculations, which showed that the phase diagram of the ^{4}He monolayer on graphene would not be affected by the ^{4}He adsorption on the other side [31]. In this paper we report a PIMC study of the ^{4}He adsorption on both sides of a single α-graphyne sheet. Because α-graphyne is more porous than graphene, ^{4}He atoms can penetrate through graphyne to allow physical exchanges among ^{4}He atoms on opposite sides. This could result in stronger interlayer correlation than the corresponding systems on graphene. We find that ^{4}He atoms in a Mott-

*ykwon@konkuk.ac.kr

insulating state form a 2D kagome lattice as a result of the interlayer correlation when the opposite-side ^{4}He layer is a $C_{4/3}$ commensurate solid, a ferromagnetic state in a pseudospin terminology. Effects of the interlayer correlation between two ferromagnetic $C_{4/3}$ solids are found to depend on the substrate potential used; the parallel and the antiparallel pseudospin alignments between two ^{4}He layers are nearly degenerate with the substrate potential based on the Lennard-Jones (LJ) ^{4}He-C pair potentials whereas the antiparallel alignment is favored with the one described by the Yukawa-6 pair potentials. The vacancy formation in a ^{4}He layer on α-graphyne is also found to be affected by the presence of the opposite-side ^{4}He layer.

In the following section, we outline our approach and some computational details. The PIMC results along with the related discussions are presented in detail in Sec. III. We summarize our findings in Sec. IV.

II. METHODOLOGY

In this study, a single α-graphyne sheet is set to be at $z = 0$. The ^{4}He-graphyne interaction is assumed to be a pairwise sum of interatomic potentials between the carbon atoms and a ^{4}He atom, which has been widely used to describe the interaction between a ^{4}He atom and a carbon substrate [6,8,9,30,31]. For the ^{4}He-C interatomic pair potential, we employ two anisotropic potentials proposed by Carlos and Cole [32,33], i.e., a 6–12 LJ potential and a Yukawa-6 potential. For the computational convenience our previous study for the ^{4}He monolayer on bilayer α-graphyne was performed with only isotropic parts of the LJ pair potential. However, the original interatomic pair potentials of Carlos and Cole include anisotropic parts to fit helium scattering data from graphite surfaces. Even though the inclusion of the anisotropic parts of the interatomic potentials has little effect on quantum phases displayed by the ^{4}He layer on one side of α-graphyne, it allows some ^{4}He atoms to be closer to the substrate, resulting in a stronger correlation between two ^{4}He layers on the opposite sides (the minima of the substrate potential made of the anisotropic pair potentials are deeper and closer to graphyne than the corresponding ones based on only isotropic parts of the pair potentials). This leads to our decision for using the substrate potentials based on fully anisotropic interatomic pair potentials, which should give a better description of the interlayer correlation. Furthermore, since the LJ and the Yukawa-6 potentials used in this study were based on an interaction between helium and sp^2-bonded carbon atoms in graphite, we tested the sensitivity of our modeling of ^{4}He-graphyne potentials to the well depth of the pair potentials. Although a decrease in the well depth yields more fluctuations in ^{4}He density distributions, the density modulations are found to change only little, and our main results presented below are still, at least qualitatively, valid. For the ^{4}He-^{4}He interaction, we use a well-known potential of Aziz *et al.* [34].

In the discrete path-integral representation, the thermal density matrix at a low temperature is expressed by a convolution of M high-temperature density matrices with an imaginary time step of $\tau = 1/(Mk_BT)$ [35]. Although the isotropic parts of ^{4}He-C pair potentials along with the ^{4}He-^{4}He potential pair potentials are used to compute the exact two-body density matrices [35,36] at the high temperature MT, their anisotropic parts are treated with the primitive approximation [35]. This is found to give an accurate description of both ^{4}He-^{4}He and ^{4}He-graphyne interactions with a time step of $(\tau k_B)^{-1} = 80$ K. We employ the multilevel Metropolis algorithm to sample the imaginary time paths along with permutations among ^{4}He atoms as described in Ref. [35]. To minimize finite-size effects, periodic boundary conditions are applied along the lateral directions.

III. RESULTS

The PIMC calculations were performed with a fixed 3×2 simulation cell with dimensions of 21.01×24.26 Å^2, the same as in our previous study for ^{4}He on bilayer α-graphyne [8]. We focus on the interlayer correlation between two ^{4}He layers on the opposite sides of graphyne, which are either in a Mott-insulating state or in a pseudospin-aligned commensurate solid state. The results obtained with two different substrate potentials, the LJ potential and the Yukawa-6 one, are presented separately below.

A. Lennard-Jones substrate potential

For PIMC calculations with the LJ substrate potential, we first prepare the α-graphyne surface whose in-plane hexagon center is occupied by a single ^{4}He atom and whose lower side is coated with a monolayer of ^{4}He atoms constituting a $C_{4/3}$ commensurate solid while each of the in-plane centers is occupied by a single ^{4}He atom. The simulations for the ^{4}He adsorptions on the upper side of the prepared graphyne surface begin from an initial configuration of ^{4}He atoms being randomly distributed at the distances far away from graphyne. Figure 1 presents one-dimensional (1D) density distributions of ^{4}He atoms as a function of the vertical coordinate z along the direction perpendicular to the graphyne surface for two

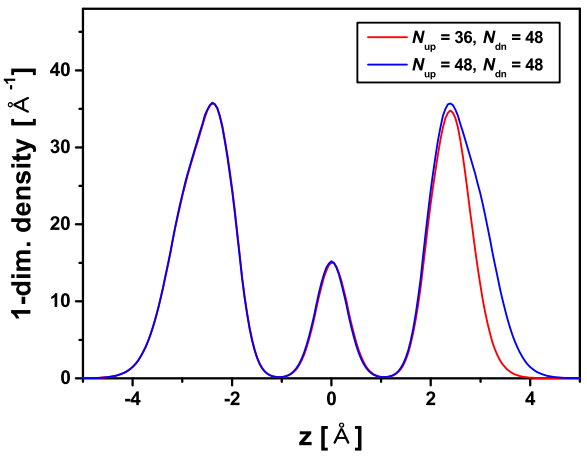

FIG. 1. (Color online) One-dimensional density distributions of ^{4}He atoms adsorbed on both sides of α-graphyne as a function of the vertical coordinate z perpendicular to the graphyne surface, which were computed with the LJ substrate potential. Here N_{up} and N_{dn} represent the number of ^{4}He atoms per 3×2 simulation cell in the upper and the lower ^{4}He layers, respectively. An additional 12 ^{4}He atoms per simulation cell are involved to form the zeroth layer around $z = 0$ where one ^{4}He atom is embedded at every hexagon center (see Ref. [8]).

different combinations of particle numbers per simulation cell. Two distinct density peaks, which correspond to the upper and the lower ^{4}He layers, are observed on the opposite sides of graphyne. Note that 36 and 48 ^{4}He atoms per simulation cell correspond to the Mott-insulating density of 0.0706 Å^{-2} and the $C_{4/3}$ commensurate density of 0.0941 Å^{-2}, respectively. The additional density peak at $z = 0$ corresponds to the zeroth layer consisting of ^{4}He atoms embedded onto the in-plane hexagon centers, which was also observed in our previous study for ^{4}He adatoms on a bilayer α-graphyne [8]. Since the peak-to-peak distance between the upper and the lower layers is estimated to be about 4.8 Å, one can expect that the van der Waals interaction between ^{4}He atoms on the opposite sides is weakly attractive (note that the potential of Aziz *et al.* we used for the ^{4}He-^{4}He interaction has a minimum value at $r \sim 3.0$ Å). In addition, the clear separation between the adjacent density peaks in Fig. 1 suggests that exchange couplings among ^{4}He atoms in different layers are nearly absent and any correlation between the upper and the lower layers, if it exists, should stem mostly from the weakly attractive ^{4}He-^{4}He interaction rather than particle exchanges.

Figure 2 shows 2D density distributions of the upper-layer ^{4}He atoms, whereas the lower-layer density peaks represented

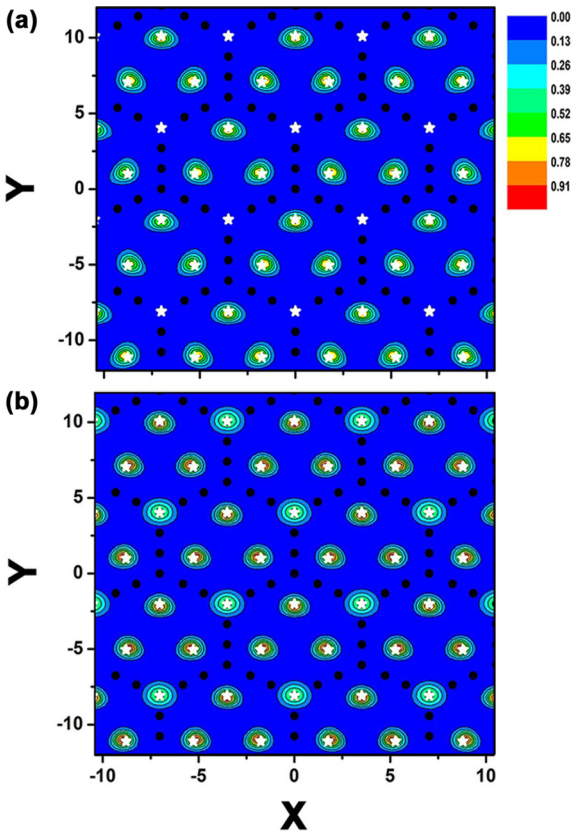

FIG. 2. (Color online) Contour plots of two-dimensional density distributions of ^{4}He atoms adsorbed on the upper side of α-graphyne for upper-layer areal densities of (a) 0.0706 Å^{-2} and (b) 0.0941 Å^{-2} (red: high; blue: low). The black dots correspond to the carbon atoms, and the white stars represent the peak positions of the lower-layer ^{4}He density distribution, which form a $C_{4/3}$ commensurate solid. The computations were performed at $T = 0.5$ K with the LJ substrate potential, and the length unit is in angstroms.

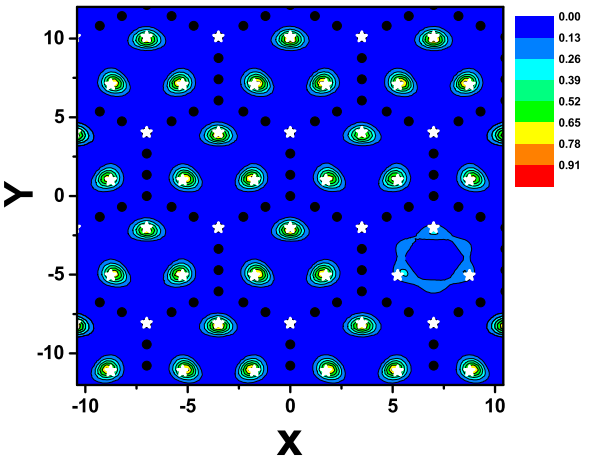

FIG. 3. (Color online) Contour plot of two-dimensional density distribution of the upper ^{4}He layer at the areal density of 0.0687 Å^{-2}, which corresponds to one less ^{4}He atoms per our 3×2 rectangular simulation cell than the Mott-insulating density (red: high; blue: low). The black dots correspond to the carbon atoms, and the white stars represent the density peaks of the lower-layer $C_{4/3}$ commensurate solid. The computations were performed at $T = 0.5$ K with the LJ substrate potential, and the length unit is in angstroms.

by the white stars constitute a $C_{4/3}$ commensurate structure with all pseudospins being in the spin-up state (see Fig. 3 of Ref. [8]). Here a distinct density peak in each plot represents an occupancy of a single ^{4}He atom. At an areal density of 0.0706 Å^{-2}, every hexagonal cell of graphyne is seen in Fig. 2(a) to accommodate three upper-layer ^{4}He atoms, which is a manifestation of a Mott-insulating state. Without the lower ^{4}He layer in a pseudospin-aligned commensurate solid state, this Mott-insulating state is a nonmagnetic spin liquid of frustrated antiferromagnets in terms of pseudospin degrees of freedom (see Fig. 2(d) in Ref. [8]). However, in the presence of the pseudospin-aligned lower ^{4}He layer, the upper-layer pseudospins are shown in Fig. 2(a) to be aligned in the same direction as the lower-layer ones. Our PIMC simulations at $T = 0.5$ K have also produced the antiparallel pseudospin alignment between the two ^{4}He layers. This is understood by the fact that the parallel alignment is energetically favored only by $\sim$0.3 K per an upper-layer helium atom over the antiparallel alignment, i.e., two pseudospin alignments are nearly degenerate. We here note that the upper-layer ^{4}He atoms in a pseudospin-aligned Mott insulating state of Fig. 2(a) constitute a 2D kagome lattice. This is also true when the upper-layer pseudospins are aligned in the opposite direction to the lower-layer ones. Therefore one can conclude that as a result of the interlayer correlation, the upper-layer ^{4}He atoms form a kagome lattice structure at the Mott-insulating density of 0.0706 Å^{-2} when the lower ^{4}He atoms constitute a pseudospin-aligned $C_{4/3}$ commensurate solid.

The interlayer correlation between two ferromagnetic $C_{4/3}$ commensurate solids is also analyzed. Figure 2(b) presents the 2D density distribution of the upper-layer ^{4}He atoms at the areal density of 0.0941 Å^{-2} where they constitute a 4/3 commensurate solid. The upper-layer pseudospins are seen to be aligned in the same direction as the lower-layer ones.

Similar to the case of the Mott-insulating state, the antiparallel pseudospin alignment was also observed in our simulations. These two pseudospin alignments are more degenerate (the parallel alignment was found to be preferred by $\sim$0.11 K per upper-layer ^{4}He atom) than the parallel and antiparallel pseudospin alignments between a Mott-insulator and a $C_{4/3}$ solid in Fig. 2(a). This can be understood by the fact that unlike ^{4}He atoms inside a hexagonal cell, upper-layer ^{4}He atoms at the vertices of the graphyne hexagons in a $C_{4/3}$ solid state prefer the other sublattice sites over the ones occupied by the corresponding lower-layer helium atoms. We note that once a pseudospin alignment between the two 4/3 commensurate ^{4}He solids is established, either parallel or antiparallel to each other, the energy barrier is too large to reverse one alignment to the other.

Now we analyze the effects of the interlayer correlation on the formation of vacancies especially in a Mott insulator with the kagome lattice structure. Figure 3 shows the 2D density distribution of 35 upper-layer ^{4}He atoms, one less than the Mott-insulating case, per 3×2 simulation cell. So the upper-layer Mott insulator contains one vacancy per simulation cell whereas the lower ^{4}He layer is the same 4/3 commensurate solid as in Fig. 2(a). One can see that every hexagonal cell, except one, is seen to accommodate three upper-layer ^{4}He atoms and its pseudospin is aligned in the same direction as those of the ferromagnetic lower layer. As shown in Fig. 3, one cell involving only two upper-layer atoms does not show the clear pseudospin alignment. This tells us that the kagome lattice structure is sustained even with the creation of vacancies but those isolated vacancies are restricted at one triangle of this trihexagonal tiling structure without hopping to the neighboring sites because of the high potential barrier provided by the graphyne surface.

The structural features described above for two ^{4}He monolayers on opposite sides of α-graphyne were also observed in the PIMC calculations for a larger system or at a lower temperature. Figure 4(a) shows the static structure factors divided by the number of ^{4}He atoms as a function of wave vector k for the upper ^{4}He layer on a single α-graphyne sheet whose lower side is coated with a $C_{4/3}$ commensurate solid as in the case of Fig. 2(a). Here, the black and the red symbols represent the PIMC results obtained with the 3×2 rectangular simulation cell at $T = 0.5$ and 0.25 K, respectively, whereas the blue symbols correspond to the results computed with the 4×3 simulation cell at $T = 0.5$ K. From the fact that the structure factor shows little change when the temperature decreases from 0.5 to 0.25 K, we conclude that the phase observed in the upper ^{4}He layer is truly a quantum phase and is hardly affected by thermal fluctuations at temperatures below 0.5 K. Furthermore, little or no difference between the PIMC results for two different system sizes suggests that the structural features presented above are not affected by the finite sizes of our systems. We note that the PIMC calculations for larger systems than ours could be performed using the worm algorithm which was introduced by Boninsegni *et al.* [37] for grand-canonical ensemble calculations.

In Fig. 4(a), one can observe the first three peaks of the upper-layer structure factors located at $k = 1.04$, 1.79, and 2.07 Å^{-1}, which is a feature of a kagome structure with the lattice constant of 7.00 Å, the lattice constant of the graphyne

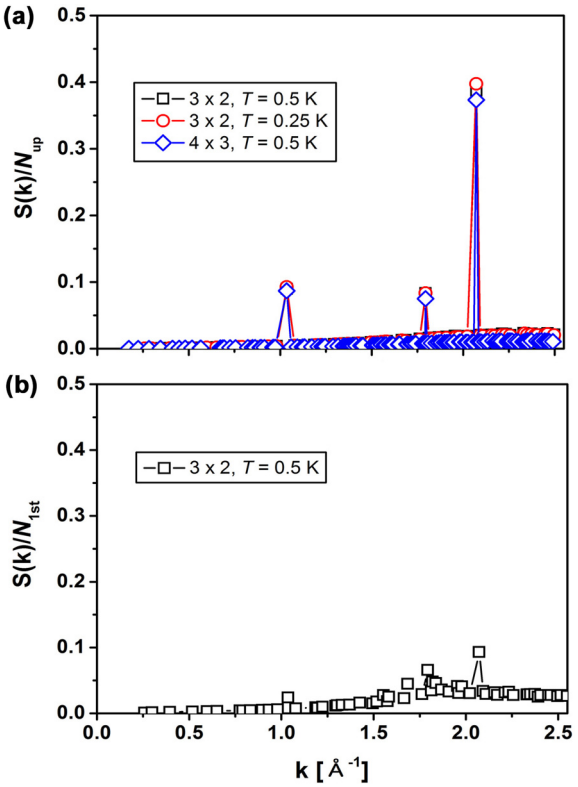

FIG. 4. (Color online) Static structure factors divided by the number of ^{4}He atoms as a function of wave vector k (a) for the upper helium layer on a single α-graphyne sheet whose lower side is coated with a $C_{4/3}$ commensurate ^{4}He solid and (b) for the first ^{4}He layer on bilayer α-graphyne without the lower ^{4}He layer. Both ^{4}He layers in (a) and (b) are at the Mott-insulating density of 0.0706 Å^{-2}. The configuration of ^{4}He atoms in (a) is the same as in Fig. 2(a) whereas the helium configuration in (b) is identical to the one for Fig. 2(d) of Ref. [8]. The black and the red symbols in (a) represent the data obtained from the PIMC calculations for the 3×2 simulation cell at $T = 0.5$ and 0.25 K, respectively, whereas the blue ones in (a) show the PIMC data for the 4×3 simulation cell at $T = 0.5$ K. The statistical errors are smaller than the symbol sizes.

substrate. This, along with the fact that the first three peak values divided by the number of the lattice points are 0.11, 0.11, and 1.00 for a perfect kagome lattice, confirms that the upper-layer ^{4}He atoms form a 2D kagome structure. The difference between the observed peak heights and the ideal ones can be attributed to quantum fluctuations of ^{4}He adatoms. On the other hand, the structure factor of the first ^{4}He layer on α-graphyne without the pseudospin-aligned $C_{4/3}$ solid on the opposite side does not show any clear peak at the Mott-insulating density of 0.0706 Å^{-2} [see Fig. 4(b)]. This is consistent with the conclusion of Ref. [8] that the Mott insulator is a nonmagnetic spin liquid in terms of pseudospin degrees of freedom. The contrast between Figs. 4(a) and 4(b) provides convincing evidence that the formation of a kagome structure in the upper ^{4}He layer is due to the interlayer correlation.

B. Yukawa-6 substrate potential

Our PIMC simulations with the Yukawa-6 substrate potential start from an initial configuration of N_{up} and N_{dn} ^{4}He atoms

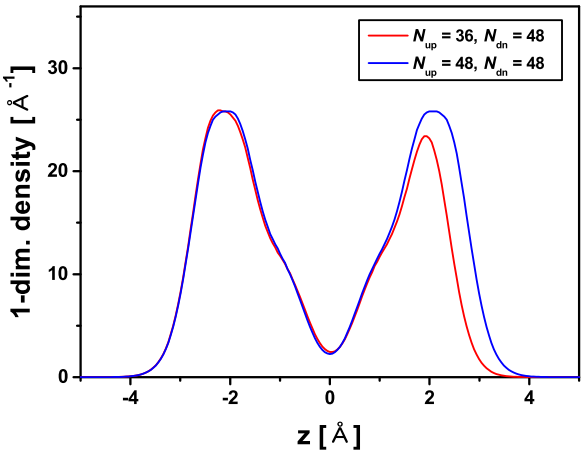

FIG. 5. (Color online) One-dimensional density distributions of ^{4}He atoms adsorbed on both sides of α-graphyne as a function of the vertical coordinate z perpendicular to the graphyne surface, which were computed with the Yukawa-6 substrate potential. Here N_{up} and N_{dn} represent the number of ^{4}He atoms per 3×2 simulation cell in the upper and the lower ^{4}He layers, respectively.

being distributed randomly on the upper and the lower sides of α-graphyne, respectively. Figure 5 presents the 1D ^{4}He density distributions as a function of the vertical coordinate z for two different values of N_{up} whereas N_{dn} is fixed to 48 per 3×2 simulation cell. Unlike Fig. 1 for the LJ substrate potential, only two density peaks on the opposite sides of graphyne are observed without the zeroth layer consisting of ^{4}He atoms embedded onto the in-plane hexagon centers. The absence of the zeroth ^{4}He layer is attributed to the fact that the Yukawa-6 substrate potential is more slowly varying near the potential minima, that is, the hexagon centers, than the LJ substrate potential. Note that the Yukawa-6 ^{4}He-C pair potential is less repulsive at short distances than the LJ interatomic pair potential [33]. The distance between the two density peaks is $\sim$4.0 Å, shorter than the corresponding distance for the LJ substrate potential. Furthermore, there is a significant overlap between the two density peaks that are broader than those in Fig. 1. This indicates large quantum fluctuations of ^{4}He adatoms along the vertical direction, which could result in frequent particle exchanges between these two layers.

Figure 6 shows 2D density distributions of the upper-layer ^{4}He atoms, whereas the lower-layer density peaks are represented by the white stars. Even with the Yukawa-6 substrate potential, the lower ^{4}He layer is seen to constitute a pseudospin-aligned $C_{4/3}$ commensurate solid at the areal density of 0.0941 Å^{-2}. This provides another confirmation to the conclusion of Ref. [8] that most of the quantum phases manifested in the ^{4}He monolayer on the α-graphyne surface, such as a Mott insulator, commensurate solids, and pseudospin degrees of freedom, are not sensitive to the specifics of the substrate potential but are determined mostly by the surface geometry. It is also shown in Fig. 6(a) that the upper-layer ^{4}He atoms under the Yukawa-6 substrate potential are in a Mott-insulating state at the areal density of 0.0706 Å^{-2} with each hexagonal cell accommodating three ^{4}He atoms. Unlike Fig. 2(a), however, all upper-layer pseudospins are aligned in

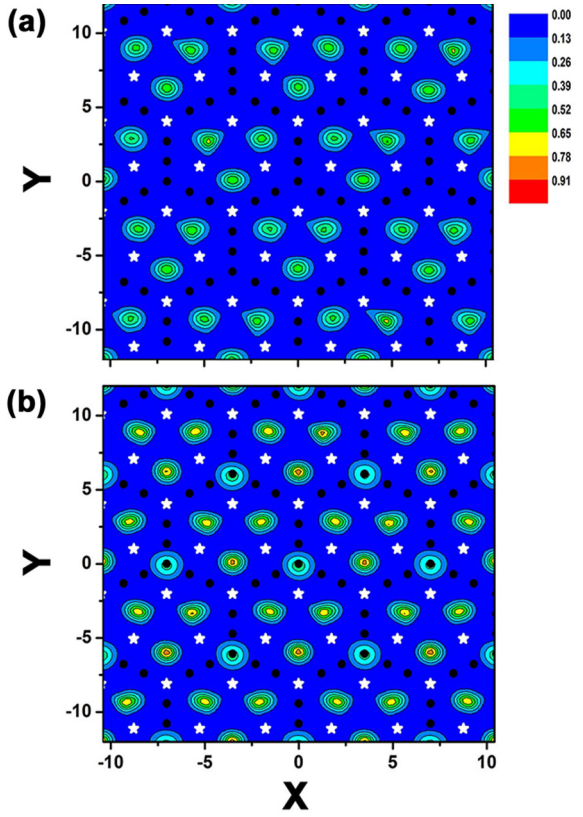

FIG. 6. (Color online) (a) Contour plots of two-dimensional density distributions of ^{4}He atoms adsorbed on the upper side of α-graphyne for upper-layer areal densities of (a) 0.0706 Å^{-2} and (b) 0.0941 Å^{-2} (red: high; blue: low). The black dots correspond to the carbon atoms, and the white stars represent the peak positions of the ^{4}He density distribution of the lower layer whose density is 0.0941 Å^{-2} for both cases. The computations were performed at $T = 0.5$ K with the Yukawa-6 substrate potential, and the length unit is in angstroms.

the opposite direction to those of the ferromagnetic lower-layer commensurate solid. We understand that the increase in the effective hard-core radii of ^{4}He adatoms due to larger quantum fluctuations along with a shorter interlayer distance cause the antiparallel pseudospin alignment to be favored under the Yukawa-6 substrate potential. As observed with the LJ substrate potential, the upper-layer ^{4}He adatoms in the pseudospin-aligned Mott-insulating state constitute a 2D kagome lattice structure. The interlayer correlation that favors the antiparallel pseudospin alignment is more evident between two ferromagnetic $C_{4/3}$ solids. We observe in Fig. 6(b) that the pseudospins of an upper-layer 4/3 commensurate solid are in a spin-down state whereas the lower-layer pseudospins are in a spin-up state. This antiparallel pseudospin alignment between the two ^{4}He adlayers corresponds to the AB stacking of two triangular solids. So we conclude that with the Yukawa-6 substrate potential, the AB stacking is preferred to the AA stacking between two $C_{4/3}$ triangular ^{4}He solids whereas these two stacking orders are nearly degenerate with the LJ potential as discussed in Sec. III A.

We now try to create a single vacancy in the upper-layer Mott insulator, i.e., the kagome lattice structure, by setting only

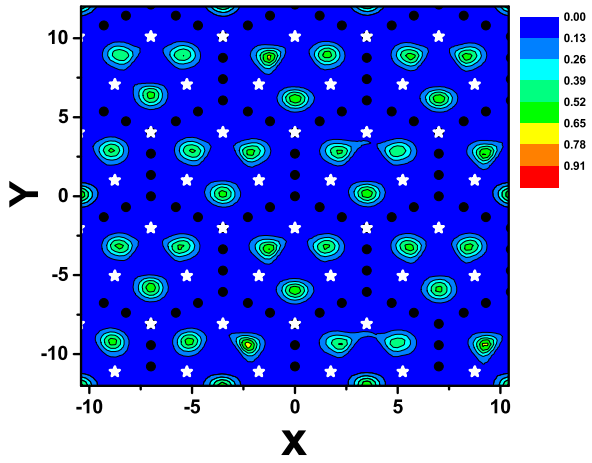

FIG. 7. (Color online) Contour plot of two-dimensional density distribution of the upper ^{4}He layer at the areal density of 0.0687 Å^{-2}, which corresponds to one less ^{4}He atoms per our 3×2 rectangular simulation cell than the Mott-insulating density (red: high; blue: low). The black dots correspond to the carbon atoms, and the white stars represent the density peaks of the lower-layer $C_{4/3}$ commensurate solid. The computations were performed at $T = 0.5$ K with the Yukawa-6 substrate potential, and the length unit is in angstroms.

35 ^{4}He atoms on the upper side in our simulation. Figure 7 presents the 2D density distribution of the upper-layer ^{4}He atoms along with the lower-layer density peaks of a pseudospin-up $C_{4/3}$ commensurate solid. It is shown that there are still three upper-layer density peaks per every hexagonal cell, corresponding to a configuration of a Mott insulator with all pseudospins being in the down state. However, one lower-layer density peak or one white star is missing at a vertex of the graphyne honeycomb structure (see the bottom right corner), which prevents the lower-layer ^{4}He atoms from forming a perfect $C_{4/3}$ triangular lattice. This suggests that when a single vacancy is created in a upper-layer kagome lattice, one lower-layer ^{4}He atom moves to the upper layer to form a perfect upper-layer lattice structure whereas a localized vacancy is created in the lower-layer 4/3 commensurate solid. This lower-layer vacancy is found at a vertex site on top of a carbon atom because it is a less favorable site for a ^{4}He adatom than a site inside a hexagonal cell. The layer-to-layer hopping of a vacancy can be understood by a short interlayer distance and large quantum fluctuations along the vertical direction under the Yukawa-6 substrate potential.

IV. CONCLUSION

According to our PIMC calculations of using two different ^{4}He-substrate potentials, ^{4}He atoms form distinct layers on both sides of a single α-graphyne sheet. Regardless of the substrate potential used, the upper-layer ^{4}He atoms form a 2D kagome structure at the Mott-insulating density of 0.0706 Å^{-2} as a result of the interlayer correlation when the lower layer is a pseudospin-aligned $C_{4/3}$ commensurate solid. Since the interaction of ^{3}He atoms with a substrate or between themselves is similar to the corresponding interaction for ^{4}He, the same kagome lattice structure is expected to be formed in the fermionic counterpart of the upper ^{4}He layer, i.e., a ^{3}He upper layer adsorbed on α-graphyne, when its lower side is coated with the $C_{4/3}$ commensurate helium solid. We speculate that some novel phenomena related with a geometrically frustrated antiferromagnetism, such as quantum spin liquids [38–40], could emerge in this ^{3}He kagome lattice.

The interlayer correlation results in different stacking orders between two $C_{4/3}$ commensurate triangular solids on the opposite sides of graphyne, depending on the substrate potential; with the Yukawa-6 potential, the AB stacking (an antiparallel pseudospin alignment between two ^{4}He solids) is found to be favored, but both AA (a parallel pseudospin alignment) and AB-stacking configurations are nearly degenerate with the LJ substrate potential. This is attributed to the difference between two substrate potentials in the interlayer distance as well as in the magnitude of quantum fluctuations along the vertical direction. A more accurate ^{4}He-graphyne potential would be required to draw a definite conclusion about the preferred stacking order of two commensurate triangular ^{4}He solids on the opposite sides of α-graphyne.

Recent theoretical studies performed by Vranješ-Markić *et al.* [30] and Gordillo [31] reported that the interlayer correlation between two ^{4}He systems adsorbed on both sides of graphene was very weak and the quantum phase diagram of one ^{4}He layer would not be affected by the presence of the opposite-side ^{4}He layer. On the other hand, our PIMC calculations have revealed some significant effects of the interlayer correlation on the structural properties of the ^{4}He monolayers on α-graphyne. This difference is understood to be due to the much more porous nature of α-graphyne than graphene.

ACKNOWLEDGMENTS

This work was supported by the Basic Science Research Program (Grant No. 2012R1A1A2006887) through the National Research Foundation of Korea funded by the Ministry of Education, Science and Technology. We also acknowledge the support from the Supercomputing Center/Korea Institute of Science and Technology Information with supercomputing resources including technical support (Grant No. KSC-2014-C3-039).

[1] G. Zimmerli, G. Mistura, and M. H. W. Chan, Phys. Rev. Lett. **68**, 60 (1992).
[2] D. S. Greywall and P. A. Busch, Phys. Rev. Lett. **67**, 3535 (1991).
[3] D. S. Greywall, Phys. Rev. B **47**, 309 (1993).
[4] P. A. Crowell and J. D. Reppy, Phys. Rev. B **53**, 2701 (1996).
[5] M. C. Gordillo and J. Boronat, Phys. Rev. Lett. **102**, 085303 (2009).
[6] Y. Kwon and D. M. Ceperley, Phys. Rev. B **85**, 224501 (2012).
[7] J. Happacher, P. Corboz, M. Boninsegni, and L. Pollet, Phys. Rev. B **87**, 094514 (2013).

[8] Y. Kwon, H. Shin, and H. Lee, Phys. Rev. B **88**, 201403(R) (2013).
[9] J. Ahn, H. Lee, and Y. Kwon, Phys. Rev. B **90**, 075433 (2014).
[10] M. W. Cole, V. H. Crespi, G. Stan, C. Ebner, J. M. Hartman, S. Moroni, and M. Boninsegni, Phys. Rev. Lett. **84**, 3883 (2000).
[11] M. C. Gordillo, Phys. Rev. Lett. **101**, 046102 (2008).
[12] Y. Kwon and H. Shin, Phys. Rev. B **82**, 172506 (2010).
[13] H. Shin and Y. Kwon, J. Chem. Phys. **136**, 064514 (2012).
[14] B. Kim and Y. Kwon, J. Low Temp. Phys. **171**, 599 (2013).
[15] S. Park and Y. Kwon, Phys. Rev. E **89**, 042118 (2014).
[16] P. Corboz, M. Boninsegni, L. Pollet, and M. Troyer, Phys. Rev. B **78**, 245414 (2008).
[17] R. H. Baughman, H. Eckhardt, and M. Kertesz, J. Chem. Phys. **87**, 6687 (1987).
[18] V. R. Coluci, S. F. Braga, S. B. Legoas, D. S. Galvão, and R. H. Baughman, Nanotechnology **15**, S142 (2004).
[19] D. Malko, C. Neiss, F. Viñes, and A. Görling, Phys. Rev. Lett. **108**, 086804 (2012).
[20] B. G. Kim and H. J. Choi, Phys. Rev. B **86**, 115435 (2012).
[21] J. Chen, J. Xi, D. Wang, and Z. Shuai, J. Phys. Chem. Lett. **4**, 1443 (2013).
[22] H. Zhang, M. Zhao, X. He, Z. Wang, X. Zhang, and X. Liu, J. Phys. Chem. C **115**, 8845 (2011).
[23] H. Hwang, Y. Kwon, and H. Lee, J. Phys. Chem. C **116**, 20220 (2012).
[24] H. Hwang, J. Koo, M. Park, N. Park, Y. Kwon, and H. Lee, J. Phys. Chem. C **117**, 6919 (2013).
[25] Y. Tobe, I. Ohki, M. Sonoda, H. Niino, T. Sato, and T. Wakabayashi, J. Am. Chem. Soc. **125**, 5614 (2003).
[26] M. M. Haley, Pure Appl. Chem. **80**, 519 (2008).
[27] F. Diederich and M. Kivala, Adv. Mater. **22**, 803 (2010).
[28] H. Shin, S. Kang, J. Koo, H. Lee, J. Kim, and Y. Kwon, J. Chem. Phys. **140**, 114702 (2014).
[29] J. C. Meyer, A. K. Geim, M. I. Katsnelson, K. S. Novoselov, T. J. Booth, and S. Roth, Nature (London) **446**, 60 (2007).
[30] L. Vranješ Markić, P. Stipanović, I. Bešlić, and R. E. Zillich, Phys. Rev. B **88**, 125416 (2013).
[31] M. C. Gordillo, Phys. Rev. B **89**, 155401 (2014).
[32] W. E. Carlos and M. W. Cole, Phys. Rev. Lett. **43**, 697 (1979).
[33] W. E. Carlos and M. W. Cole, Surf. Sci. **91**, 339 (1980).
[34] R. A. Aziz, M. J. Slaman, A. Koide, A. R. Allnatt, and W. J. Meath, Mol. Phys. **77**, 321 (1992).
[35] D. M. Ceperley, Rev. Mod. Phys. **67**, 279 (1995).
[36] R. E. Zillich, F. Paesani, Y. Kwon, and K. B. Whaley, J. Chem. Phys. **123**, 114301 (2005).
[37] M. Boninsegni, N. Prokof'ev, and B. Svistunov, Phys. Rev. Lett. **96**, 070601 (2006).
[38] L. Balents, Nature (London) **464**, 199 (2010).
[39] T.-H. Han, J. S. Helton, S. Chu, D. G. Nocera, J. A. Rodriguez-Rivera, C. Broholm, and Y. S. Lee, Nature (London) **492**, 406 (2012).
[40] M. Punk, D. Chowdbury, and S. Sachdev, Nat. Phys. **10**, 289 (2014).